International Journal on Advanced Science Engineering Information Technology

Vol.12 (2022) No. 1
ISSN: 2088-5334

Characterization of the Urethane Based Tissue Equivalent Substitute for Phantom Construction: Model Molding, XCOM and MCNPX Studies

Olaseni M. Bello [a,b,*], Norehan M. Nor [a], Wan Muhamad S. Wan Hassan [a]

[a] *Department of Physics, Universiti Teknologi Malaysia, UTM, Johor Bahru, 81310, Johor, Malaysia*
[b] *Department of Physics, Nigeria Police Academy, Wudil, Kano, 71310, Nigeria*
Corresponding Author: [*] olaseni@graduate.utm.my

***Abstract*— The Soft and Lung tissue equivalent substitute (STES and LTES) were developed from urethane PMC121/30 Dry (A and B) of Smooth-On, USA. The part A and B were mixed in the ratio 1:1 and further mixed with calcium carbonate ($CaCO_3$) at a ratio 2:1 by mass. Air moisture was extracted from the mixture for 10minutes. This is the STES and the density after air extraction was 1.04gcm^{-3}. The LTES was developed by mixing the STES and polystyrene beads at a ratio 10:1 by mass. The density of the LTES was 0.25gcm^{-3} after air extraction. The STES and the LTES were subjected to compression test for stress-strain analysis. The elemental composition of STES and LTES was achieved using XCOM software with the IUPAC nomenclatures of the source compounds as inputs. The elemental composition obtained was used to modify the lung and the soft tissue material of the AMALE and AFEMALE computational phantom of ORNL. The phantom was subjected to photon exposure (0.06MeV-15.00MeV) using MCNPX Version 27e. The results from MCNPX provided the bremsstrahlung, positron annihilation, and the fluorescence energies that was used to estimate the g-factor. The mass-energy transfer coefficient (μ_{tra}/ρ) and the mass-energy absorption coefficient (μ_{en}/ρ) were calculated using the values of g-factor, the fluence and the Kerma. The μ_{en}/ρ of the tissue-equivalent agrees with the National Institute of Standard values and the ICRU 44. The STES and LTES are technically proper research and teaching models for dose measurements with these results.**

***Keywords*— Tissue equivalent; MCNPX; XCOM; LTES; STES; urethane; phantom.**

Manuscript received 26 Nov. 2020; revised 21 May 2021; accepted 9 Jun. 2021. Date of publication 28 Feb. 2022.

I. INTRODUCTION

Radiation dose to the body increases with incident radiation energy during diagnostic or radiotherapy procedures, nuclear medicine, or in the event of radiation accident [1]. The energy absorbed constitutes a radiation dose to various parts of the body, the magnitude of the dose depends on the magnitude of the radiation energy absorbed. Therefore, there is a need to keep this dose under check and as low as reasonably achievable to minimize biological damage to the body. A radiation planning procedure is put in place to address this concern and put the situation under safety control. Radiation planning is pre-examining the actual procedure with tissue-like materials to ascertain the safety and appropriate energy range before subjecting the human body to the radiation procedure. This tissue-like material is referred to as the tissue-equivalent substitutes. They are developed into a complete structure to serve as a surrogate for the human body or represent an organ in the body. The surrogate is referred to as an anthropomorphic phantom. The phantoms are meant to simulate tissues such as the bone, soft and the lungs [2]. Anthropomorphic phantoms have gained recognition in radiation science, and it is an acceptable representation of the physical and dosimetric behaviors of the human body. It has been extremely useful and effective in the planning exercises of radiotherapy procedures. Planning is very relevant in the optimization of medical imaging modalities [3], [4] and also in cancer research and medical imaging-related studies [5], [6].

A. Tissue Equivalent Substitutes

The Tissue equivalent substitutes are materials with radiological properties like the human tissues they are meant to mimic [7], [8]; such properties include mong the mass density and the mass-energy absorption coefficient. The need for human tissue equivalent substitutes is on the increase [9] because tissue-equivalent substitutes are very relevant in the construction of radiation phantoms [10], [11], and it useful in

the treatment and management of damaged tissues and skin [12]. They are applicable in quality control routine, quality assurance in therapeutic and diagnostic procedures, research, and measurement of doses received by patients during medical examinations [13]. Investigating different tissue equivalent substitutes is essentially to develop radiation phantom for teaching, training, and research [14].

The construction of anthropomorphic phantoms from tissue equivalent materials is costly[15], but several tissue equivalent materials are under investigation, and report to confirm that there is progress in achieving qualitative research output at a reduced time, cost [16], [17], and improved understanding of diseases [18]. For instance, the compound of paraffin wax and sodium chloride (common salt) has been proposed for use as an equivalent material for soft tissue [19], combination of paraffin wax and other cost-effective items have also proven to be of relevant tissue-equivalent properties[20]. Polyvinylpyrrolidone (PVP) was reported [21] to have dielectric properties equivalent to soft tissue. Nylon-12 have been used as water equivalent solid phantom, and the characterization was reported [22]. Plaster of Paris, PoP was used to mimic the pediatric bone while polymethyl methacrylate, PMMA was used as the soft tissue equivalent[15]. Organic tissue cultured skin has been in use as a tissue-equivalent material [23], [24]. Using the decellularized dermal template in self-assembled skin substitute is also reported to be effective on mice[25]. Report confirmed 3D printing of a cellularized equivalent substitute for skin [26] and 3D printing of polycarbonate as a thyroid substitute [27]. The mixture of Different categories of modifiers with distilled water has been used to produce equivalent tissue [28]. Synthetic gelatins is also relevant in soft tissue simulation [29]. Skin repair of a pre-mature newborn was achieved using a bioengineered tissue substitute called Apligraf [30]. The bone tissue substitute from epoxy mixed with calcium phosphate and calcium carbonate is also reported [31]. Synthetic polymers have also been used to develop hydrogel phantoms which are used for radiation dosimetry and therapy [32]. Several efforts are in progress to produce a reliable tissue equivalent substitute, these includes the prospect of using Nano-materials as tissue equivalent substitutes [33].

Different parameters have been used to classify tissue-equivalent materials. These parameters include mass attenuation coefficient [27], Kerma factor [34], dielectric properties[21], mass density (ρ) [35], [36], effective electron density (Neff) [36], effective atomic number (Zeff), photon mass energy-absorption coefficient (μ_{en}/ρ), photon mass attenuation coefficient (μ/ρ), the total stopping power of electrons (S/ρ)tot, the absorbed depth dose [36] and the build-up parameters of the tissue-equivalent [37]. Considering Kerma factors and agreement with water equivalence, natural rubber was found to be most appropriate as soft tissue equivalent[34].

This study developed the equivalent tissue substitute from the urethane material PMC 121/30 Dry of Smooth-On, USA [10], [38]. The soft tissue equivalent substitute (STES) and the lung tissue equivalent substitute (LTES) produced in this study mimic the stomach and the lung.

B. g-factor, Mass Energy-Transfer Coefficient (μ_{tra}/ρ) and Mass Energy Absorption Coefficient (μ_{en}/ρ

This fraction of energy accounts for the lost energy due to radiative processes, especially bremsstrahlung [39] but explicitly asserts that bremsstrahlung, positron annihilation, fluorescence, knock-on electron, and energy loss straggling are to be considered in the estimation of the g-fraction [40]. In this study and within the range of the energy bin studied, bremsstrahlung, positron annihilation, and fluorescence were used to estimate the g-factor. Mass energy transfer coefficient is a measure of the energy transferred to the secondary electron due to the initial interactions [39], and it is the intermediary factor in the estimation of the mass-energy absorption coefficient[40]. The mass-energy absorption coefficient accounts for radiation emission when charged particles pass through a medium[40]. This study is meant to characterize the radiological properties of the soft and lung tissue substitutes made from urethane rubber material and set up the tissue equivalencies of the substitute materials.

II. Material and Method

The preparation of the tissue-equivalent materials is the first part. The materials used for the soft tissue equivalent substitute (STES) are the PMC 121/30 Dry parts A and B, and Calcium Carbonate ($CaCO_3$) [41]. The lung tissue equivalent substitute (LTES) is the mixture of the STES and polystyrene beads. The second part is the use of XCOM software to determine the elemental composition of the STES and LTES. The third part is the input of the elemental composition of the STES and LTES obtained from XCOM software into the MCNP code to modify the lung and the stomach of the AMALE and AFEMALE computational phantom of ORNL. Figure 1 provides the details.

A. STES and LTES Model

For the soft tissue equivalent substitute, equal volume of part A and part B of the PMC 121/30 Dry was thoroughly mixed and calcium carbonate was added at a ratio of 2 part by mass of PMC 121/30 Dry mixture to 1 part of the calcium carbonate. The mixture was thoroughly mixed and kept in air extractor for ten minutes. This is to extract the air bubbles trapped in the liquid during mixing. Two cement work was made initially to mold the stomach on both sides. The STES mixture was transferred into the hollow part of the mold, and it was allowed for 48hours to set. The lung tissue equivalent substitute was obtained by mixing ten parts by mass of the STES material with one part by mass of polystyrene beads. The mixture was mixed thoroughly and kept in the air extractor chamber for ten minutes, as in the case of the STES. The polystyrene compromised the density of the STES. The LTES was transferred into the hollow part of the lung cement mold and kept for 48hours to ensure it was properly set. The stress-strain values of the tissues were noted.

B. XCOM Software and the MCNPX

The IUPAC name of the constituent compounds of the STES and LTES materials were used as input into the XCOM software to obtain the elemental composition of the STES and LTES materials, and also the projected photon loss energies of the materials. The densities of the STES and LTES are achieved using the basic mechanical approach in the

laboratory. The elemental composition and the densities of organs impact the dose distribution[42]. The MCNP computational code files of the phantom AMALE and AFEMALE of ORNL were modified. The source used was changed to I-192, and the densities for the lung and the soft tissue were adjusted accordingly. Some tallies and dose cards were added with an enhanced NPS power ratio. The elemental material composition for the soft and the lung tissue was completely changed to that of the urethane tissue equivalent obtained in this study. The phantom radiation geometry is AP at 1m from the source.

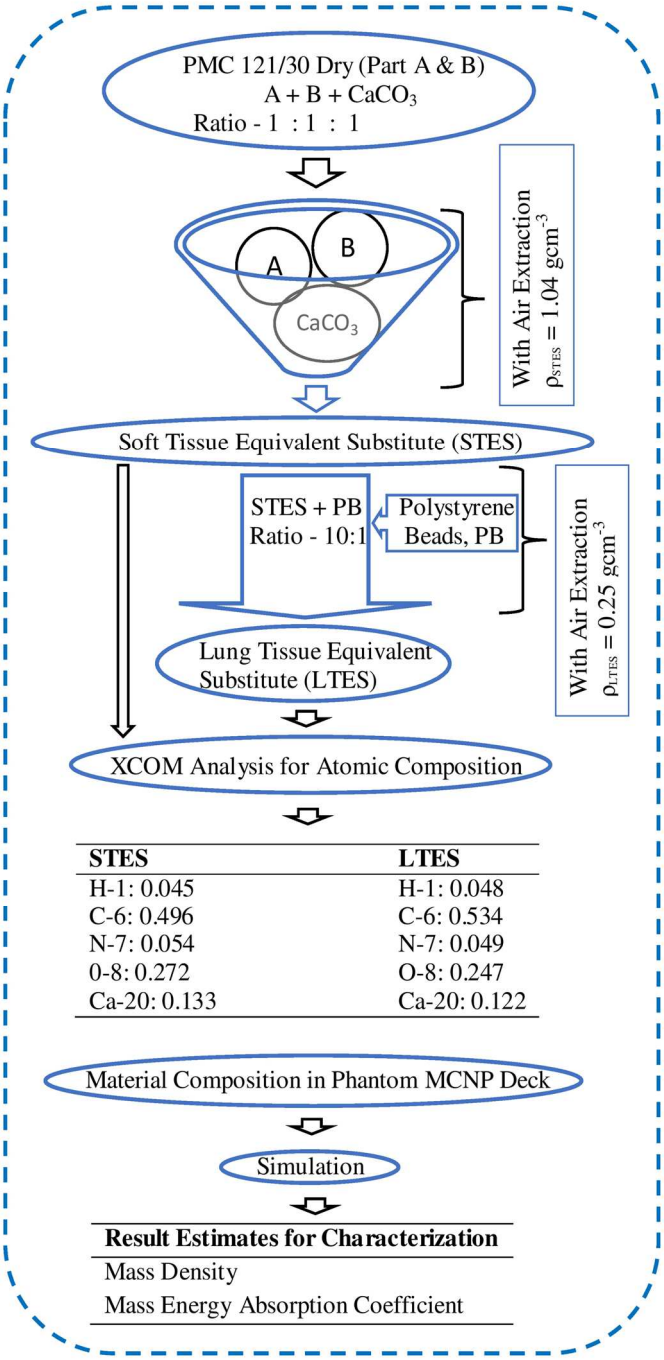

Fig. 1 Schematic representation of the method and result

C. Calculation of Mass Energy Absorption Coefficient (μ_{en}/ρ)

The mass energy absorption coefficient calculation in this study was achieved in three steps. First, the g-factor was obtained as a fraction of the sum of the bremsstrahlung, positron annihilation, and the photon energy fluorescence. Secondly, the mass-energy transfer coefficient was estimated using the MCNPX result data for each energy bin sampled, given by the quotient, Kerma by photon energy fluence. The mass-energy absorption was calculated from the values of the g-factor and the mass-energy transfer coefficient. The relative error from simulation in the fluence and the Kerma used in the calculation of the mass-energy transfer coefficient was maintained at 0.05 (5%) using a high NPS value in the

simulation. These relative errors were used to calculate the errors in the mass energy transfer coefficient values.

III. Results and Discussion

A. Elemental Composition

The elemental composition obtained from XCOM software is as presented in Table I. The soft tissue consists of 4.5% hydrogen, 49.6% carbon, 5.4% nitrogen, 27.2% oxygen and 13.3% calcium. Similarly, the lung tissue consists of 4.8% hydrogen (0.3% greater than the value for the soft tissue), 53.4% carbon (3.8% greater than the value for the soft tissue), 4.9% nitrogen (0.5% less than the value for the soft tissue), 24.7% oxygen (2.5% less than the value for soft tissue) and 12.2% calcium (1.1% less compared to the value for the soft tissue). The soft tissue developed in this study has more hydrogen and carbon atoms and less nitrogen, oxygen, and calcium atoms than the lung tissue developed in this study. Materials rich in calcium, carbon, hydrogen, and oxygen are the most effective tissue-equivalent substitute [7]. The density, ρ of the soft tissue equivalent substitute, STES is 1.04 $gcm^{-3,}$ while the density, ρ of the lung tissue equivalent substitute, LTES is 0.25 gcm^{-3}. According to[43], the densities of the lung and the soft tissues are approximately equal to 0.3 gcm^{-3} and 1.0 $gcm^{-3,}$ respectively. This confirmed the relevance and the reliability of the mass density obtained in this study for the developed soft and lung tissue.

TABLE I
STES AND LTES ELEMENTAL COMPOSITION

	H-1	C-6	N-7	O-8	Ca-20
STES	0.045	0.496	0.054	0.272	0.133
LTES	0.048	0.534	0.049	0.247	0.122

B. Discussion

Mass density and mass-energy absorption coefficient are used in this study to characterize the STES and the LTES. During the molding process, manual mixing was used, so air bubbles in the mixture were expected. Some samples were allowed to be set without passing them through the air extractor, while a larger part was subjected to air extraction. For the STES, the density of the sample that was not subjected to air extraction was an average of 1.40 $gcm^{-3,}$ while the average density of the sample that was subjected to air extraction was 1.04 gcm^{-3}. A similar trend was observed for LTES, but the average density of the sample that was subjected to air extraction was 0.25 gcm^{-3}. These results agree perfectly with the result from [44], with a density of 1.041 gcm^{-3} for the soft tissue. The result from this study was enhanced with the use of air extractor to extract the air bubbles trapped in the materials during mixing. It was observed that even if the mixture is machine mixed, air extraction is essential in achieving a reliable mass density result. Comparing the result of the elemental composition of the STES and the LTES; and because the addition of the polystyrene beads to the STES was just to compromise the density of the STES. The molecules of hydrogen in LTES increase by 6.67% more than the hydrogen molecules in the STES.

Similarly, carbon molecules increased by 7.66%. On the contrary, 9.26% reduction was observed in nitrogen molecules, oxygen molecules reduced by 9.19% and calcium molecules reduced by 8.27%. The details of the fractional composition of the STES and LTES are presented in Table I. Bremsstrahlung, positron annihilation, first fluorescence, and the second fluorescence constitute photon creation events recently investigated [45] that were used in the calculation of the g-factor [40]. The bremsstrahlung and first fluorescence values were consistent within the energy bins used in this study, but second fluorescence and positron annihilation recorded zero values until the source energy was 0.078MeV and 1.25MeV, respectively (refer to Appendix A). The values of the g-factor are shown in appendix A but modified in Table II for easy comparison with NIST dataset, and Figure 2 represents its behavior`.

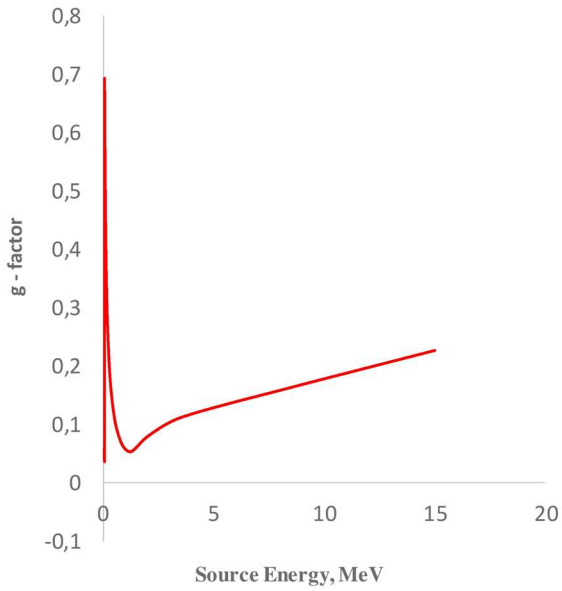

Fig. 2 Graph of g-factor vs energy

Table II is a modified Table extracted from the detailed raw data available in appendix A. Contrary to the view of [39] that assert that the g-factor is zero within the diagnostic energy range, the values obtained in this study confirmed the values are not zero. The minimum value of the g-factor estimated was 0.03642 at 0.076MeV, and it rose to the maximum value of 0.6917 at 0.078MeV when the second fluorescence recorded its first stable value. The value of the g-factor reduces to the second-lowest point of 0.0533 at 1.25MeV. The significance of the 1.25MeV is that, at this energy point, the positron annihilation, a factor in the calculation of the g-factor, recorded its first value. The g-factor rises again after the 1.25MeV energy point. The overall mean value of the g-factor recorded was 0.31271 for the energy range 0.06MeV to 15.0MeV. Within this energy range (0.06MeV to 15.0MeV), the g-factor curve exhibited one sharp peak value at 0.078MeV, two low-point values at 0.06MeV and 1.25MeV, it increases linearly afterwards. The detailed raw data is available in Appendix A.

The values of the mass-energy transfer coefficients (not shown) are derived directly from the fluence, and the Kerma obtained from the MCNP results. These two variables have a different relative error in their theoretical estimation from simulation, and these are appropriated in the calculations of the mass-energy transfer coefficients. These errors are shown

in Figure 4 for the lung and Figure 6 for the soft tissue. They are considered very important because they determine the reliability of the mass energy absorption coefficient values. It was observed for the LTES, within the diagnostic energy range (0.06 - 0.15 MeV), the error range is 0.077≥RE≥0.029 while it is 0.029≥RE≥0.003 within the radiotherapy energy range (0.15 - 15.00MeV). For the soft tissue equivalent, the error is 0.071≥ RE≥0.036 within the diagnostic energy range (0.06 - 0.15 MeV) and 0.036 ≥RE≥0.003 within the radiotherapy range (0.15 - 15.00 MeV). According to Monte Carlo N-Particle code criteria, these error ranges provide reliable results: they are < 0.05%.

The mass-energy absorption coefficients were derived from the mass-energy transfer coefficient and the g-factor using equation 3. The mass-energy absorption coefficient, μ_{en}/ρ is presented in Table II with the errors in parentheses. Table II compares the values of the mass-energy absorption coefficient for the lungs and the soft tissue. Figure 3 and Figure 5 represent the comparative curve of the mass-energy absorption coefficients, μ_{en}/ρ for the LTES and the STES, respectively, achieved in this study with the values from the National Institute of Standard and Technology (NIST). For energies 0.06MeV to 1.25MeV, the mass-energy absorption coefficients, μ_{en}/ρ for the STES, are greater than that of the LTES by an average of 5.24% of the LTES value the two values are approximately equal for energies greater than 1.25MeV. The values of mass energy-absorption coefficients, μ_{en}/ρ for the tissue substitutes, compared with the values of National Institute of Standard, NIST. The curves, figure 3 and figure 5 show a good agreement between the tissue substitutes and the NIST curve.

TABLE II
MASS ENERGY ABSORPTION COEF. (μ_{en}/ρ) FOR TISSUE SUBSTITUTE

Source Energy MeV	g-factor	This Study (Relative Error in %) LTES-μ_{en}/ρ	This Study (Relative Error in %) STES-μ_{en}/ρ
0.06	0.0423	0.170(7.63%)	0.177(7.08%)
0.08	0.675	0.033(6.11%)	0.035(6.97%)
0.10	0.543	0.031(4.84%)	0.033(5.84%)
0.15	0.367	0.023(2.90%)	0.024(3.67%)
0.20	0.280	0.021(1.92%)	0.021(2.46%)
0.30	0.193	0.019(1.07%)	0.019(1.39%)
0.40	0.147	0.019(0.71%)	0.019(0.93%)
0.50	0.116	0.019(0.54%)	0.019(0.71%)
0.60	0.096	0.019(0.46%)	0.18(0.59%)
0.80	0.071	0.018(0.38%)	0.018(0.48%)
1.00	0.058	0.017(0.34%)	0.017(0.43%)
1.25	0.053	0.017(0.32%)	0.016(0.40%)
1.50	0.060	0.016(0.31%)	0.015(0.38%)
2.00	0.079	0.014(0.29%)	0.014(0.37%)
3.00	0.103	0.011(0.28%)	0.011(0.36%)
4.00	0.118	0.009(0.28%)	0.009(0.35%)
6.00	0.139	0.007(0.29%)	0.007(0.36%)
8.00	0.159	0.005(0.29%)	0.005(0.36%)
10.00	0.178	0.004(0.29%)	0.004(0.37%)
15.00	0.227	0.002(0.31%)	0.002(0.37%)

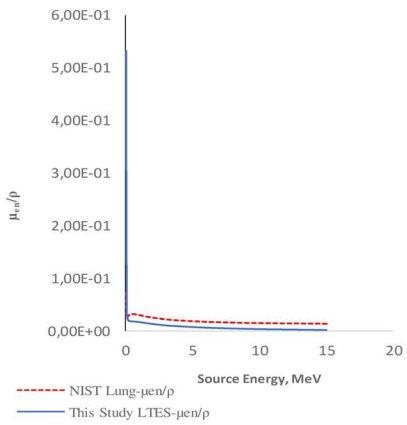

Fig. 3 Graph of μ_{en}/ρ (LTES) vs Photon Energy

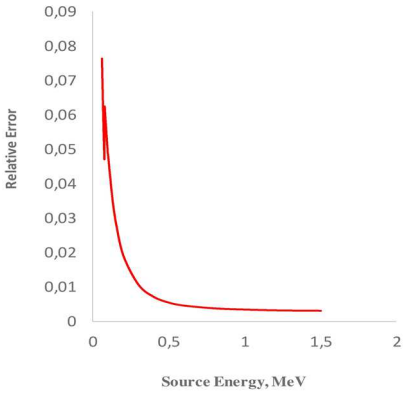

Fig. 4 Graph of Relative Error in μ_{en}/ρ (LTES) vs Energy

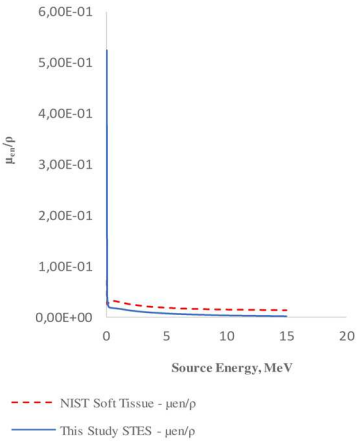

Fig. 5 Graph of μ_{en}/ρ (STES) vs Energy

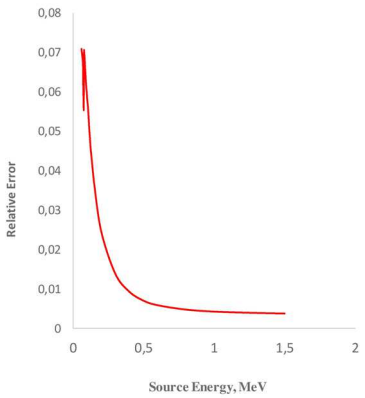

Fig. 6 Graph of Relative Error in μ_{en}/ρ (STES) vs Energy

The strong agreement between the values achieved for the mass density and the mass-energy absorption coefficient in this study and the published data of the International Commission on Radiological Protection and the National Institute of Standard and Technology, NIST confirmed that the material used in this study is a reliable tissue-equivalent substitute.

The STES and the LTES were further subjected to a compression test, Table III. The maximum load the STES can withstand is about three times that of the LTES. Similarly, the maximum strain of LTES is about four times that of the STES and the maximum stress of the STES is about thirty-three times that of the LTES. The young modulus of the STES is about one hundred and eighty times the young modulus of the LTES.

TABLE III
STES AND LTES COMPRESSION STRESS AND STRAIN

	Max. Load, N	Extension, mm	Strain	Stress, MPa	Modulus, MPa
STES	11474.188	4.00001	0.50000	2.02206	8.98708
LTES	393.783	17.50008	2.18751	0.06940	0.04818

Equations

$$g = \frac{b+pa+f1+f2}{E} \quad (1)$$

$$\text{Kerma, K} = \varphi \text{E} \left(\frac{\mu_{tr}}{\rho}\right) \quad (2)$$

$$\frac{\mu_{en}}{\rho} = \frac{\mu_{tr}}{\rho}(1-g) \quad (3)$$

$$\text{Strain} = \frac{Extension}{Original\ Length} \quad (4)$$

$$\text{Stress} = \frac{Force}{Area} \quad (5)$$

$$\text{Young Modulus} = \frac{Stress}{Strain} \quad (6)$$

$$RE_{\mu_{tra}} = \sqrt[2]{(\varphi_{RE})^2 + (K_{RE})^2} \quad (7)$$

IV. CONCLUSIONS

The mass density and the mass-energy absorption coefficients of the lung and soft tissue equivalent substitutes developed in this study were used to characterize their tissue equivalency. The achieved mass energy absorption coefficient agreed with the National Institute of standard and Technology results. The mass densities of the tissues also agree with the recommended values specified by International Commission on Radiological Protection, ICRP publication 74, and it perfectly agreed with established results. Therefore, it is reasonable to state that the tissue-equivalent substitutes developed in this study and their corresponding atomic compositions are suitable for teaching and research purposes. Recommendations: The major elemental composition recommended for the development of the soft and the lung tissue was used in this study. Future improvement in this study can be achieved by introducing sources of other minor elements like magnesium, sodium, and potassium to the soft and lung tissue composite materials at the mixture stage. It is also pertinent to further this study with the development of the bone tissue to complete the development of the whole-body radiation phantom.

NOMENCLATURE

g	g-factor	
b	Bremsstrahlung	MeV
Pa	Positron Annihilation	MeV
F1	First Fluorescence	MeV
F2	Second Fluorescence	MeV
E	Energy	MeV
K	Kerma	Gy
LTES	Lung Tissue Equivalent Substance	
STES	Soft Tissue Equivalent Substitute	
ICRU	International Commision for Radiological Units and Measurements	

Greek letters

φ	Fluence	pcm^{-2}
$\frac{\mu_{tr}}{\rho}$	Mass Energy Transfer Coefficient	$cm^2\ g^{-1}$
$\frac{\mu_{en}}{\rho}$	Mass Energy Absorption Coefficient	$cm^2\ g^{-1}$

Subscripts

tra	transfer
en	energy

ACKNOWLEDGMENT

TETFund Nigeria provided support for the PhD program and TWAS-COMSTECH Joint Research Grant provided funds for books and a computer system.

REFERENCES

[1] F. Paquet, M. R. Bailey, R. W. Leggett, and J. D. Harrison, "Assessment and interpretation of internal doses: uncertainty and variability," *ICRP 2015 Proceedngs*, pp. 202–214, 2015. https://doi.org/10.1177/0146645316633595.

[2] M. A. Alsadig, A.A., Abbas, S., Kandaiya, S., Ashikin, N.A.R.N.N., Qaeed, "Differential dose absorptions for various biological tissue equivalent materials using Gafchromic XR-QA2 film in diagnostic radiology," *Appl. Radiat. Isot.*, vol. 129, pp. 130–134, 2017. https://doi.org/10.1016/j.apradiso.2017.08.021.

[3] P. Amini, I., Akhlaghi, P., Sarbakhsh, "Construction and verification of a physical chest phantom from suitable tissue-equivalent materials for computed tomography examinations," *Radiat. Phys. Chem.*, vol. 150, pp. 51–57, 2018. https://doi.org/10.1016/j.radphyschem.2018.04.020.

[4] S. Chan, K. Dittakan, and M. Garcia-constantino, "Image Texture Analysis for Medical Image Mining: A Comparative Study Direct to Osteoarthritis Classification using Knee X-ray Image," *Int. J. Adv. Sci. Eng. Inf. Technol.*, vol. 10, no. 6, pp. 2189–2199, 2020. https://doi.org/10.18517/ijaseit.10.6.8279.

[5] H. Tony and C. Apriono, "Design of THz High-Resistivity Silicon-Based Microstrip Antenna for Breast Cancer Imaging," *Int. J. Adv. Sci. Eng. Inf. Technol.*, vol. 10, no. 6, pp. 2640–2648, 2020. https://doi.org/10.18517/ijaseit.10.6.12887.

[6] A. A. Alshehri, T. Daws, and S. Ezekiel, "Medical Image Segmentation Using Multifractal Analysis," *Int. J. Adv. Sci. Eng. Inf. Technol.*, vol. 10, no. 2, pp. 420–429, 2020.

[7] A. A. Bakri and Nik Noor Ashikin Nik Ab Razak, "Characterization of Low-Cost Materials as Human Tissue Equivalent Materials," *Asian J. Appl. Sci. (ISSN*, vol. 07, no. 04, pp. 456–460, 2019.

[8] C. K. Mcgarry *et al.*, "Tissue Mimicking Materials for Imaging and Therapy Phantoms: Topical Review," *Phys. Med. Biol.*, vol. 65, no.

23TR01, 2020. https://doi.org/10.1088/1361-6560/abbd17.
[9] C. E. Ghezzi, B. Marelli, F. G. Omenetto, J. L. Funderburgh, and D. L. Kaplan, "3D Functional Corneal Stromal Tissue Equivalent Based on Corneal Stromal Stem Cells and Multi-Layered Silk Film Architecture," *PLoS One*, vol. 12(1): e01, pp. 1–18, 2017. https://doi.org/10.1371/journal.pone.0169504.
[10] J. F. Winslow, D. E. Hyer, R. F. Fisher, C. J. Tien, and D. E. Hintenlang, "Construction of anthropomorphic phantoms for use in dosimetry studies," *J. Appl. Clin. Med. Phys.*, vol. 10, no. 3, pp. 195–204, 2009. https://doi.org/10.1120/jacmp.v10i3.2986.
[11] S. F. Monzari, G. Geraily, T. Hadisi Nia, H. Toolee, and M. Farzin, "Fabrication of anthropomorphic phantoms for use in total body irradiations studies," *J. Radiother. Pract.*, vol. 19, no. 3, pp. 242–247, 2020. https://doi.org/10.1017/s1460396919000591.
[12] H. Savoji, B. Godau, M. S. Hassani, and M. Akbari, "Skin Tissue Substitutes and Biomaterial Risk Assessment and Testing," *Front. Bioeng. Biotechnol.*, vol. 6, no. July, pp. 1–18, 2018. https://doi.org/10.3389/fbioe.2018.00086.
[13] A. K. Jones, D. E. Hintenlang, and W. E. Bolch, "Tissue-equivalent materials for construction of tomographic dosimetry phantoms in pediatric radiology," *Med. Phys.*, vol. 30, no. 8, pp. 2072–2081, Aug. 2003. https://doi.org/10.1118/1.1592641.
[14] S. Medeiros, O. Ramos, M. Bárbara, T. Berdeguez, L. V. De Sá, and S. Augusto, "Anthropomorphic phantoms-potential for more studies and training in radiology," *Int. J. Radiol. Radiat. Ther.*, vol. 2, no. 4, pp. 101–104, 2017. https://doi.org/10.15406/ijrrt.2017.02.00033.
[15] A. Mohammed Ali, A., Hogg, P., Johansen, S., England, "Construction and validation of a low-cost paediatric pelvis phantom," *Eur. J. Radiol.*, vol. 108, pp. 84–91, 2018. https://doi.org/10.1016/j.ejrad.2018.09.015.
[16] M. Monzari, S.F., Geraily, G., Hadisi Nia, T., Toolee, H., Farzin, "Fabrication of anthropomorphic phantoms for use in total body irradiations studies," *J. Radiother. Pract.*, vol. 19, no. (3), pp. 242–247, 2020. https://doi.org/10.1017/s1460396919000591.
[17] A. Rafiq, M. Abu, A. Faisal, D. Cahyani, and R. Sari, "An Easily Made, Low-Cost , Bone Equivalent Material Used in Phantom Construction of Computed Tomography," *Int. J. Appl. Eng. Res.*, vol. 13, no. 10, pp. 7604–7609, 2018..
[18] J. A. Smith, A., Huang, M., Watkins, T., Baskin, J., Garlick, "De novo production of human extracellular matrix supports increased throughput and cellular complexity in 3D skin equivalent model," *J. Tissue Eng. Regen. Med.*, vol. 14, no. (8), pp. 1019–1027, 2020. https://doi.org/10.1002/term.3071.
[19] R. Zainon, N. A. B. Amin, and A. A. Tajuddin, "Establishment of paraffix wax compound and NaCl as soft-tissue equivalent material for phantom fabrication," *ASM Sci. J.*, vol. 12, no. Special Issue 3, 2019.
[20] D. Shrotriya, R. S. Yadav, R. N. L. Srivastava, and T. R. Verma, "Design and development of an indigenous in-house tissue-equivalent female pelvic phantom for radiological dosimetric applications," *Iran. J. Med. Phys.*, vol. 15, no. 3, 2018. 10.22038/ijmp.2018.26717.1274.
[21] R. Ianniello, C., de Zwart, J.A., Duan, Q., Lattanzi, R., Brown, "Synthesized tissue-equivalent dielectric phantoms using salt and polyvinylpyrrolidone solutions," *Magn. Reson. Med.*, vol. 80, no. (1), pp. 413–419, 2018. https://doi.org/10.1002/mrm.27005.
[22] F. C. P. Ade, N., van Eeden, D., du Plessis, "Characterization of Nylon-12 as a water-equivalent solid phantom material for dosimetric measurements in therapeutic photon and electron beams," *Appl. Radiat. Isot.*, vol. 155, no. 108919, 2020. https://doi.org/10.1016/j.apradiso.2019.108919.
[23] N. Zoller *et al.*, "Assessment of melanogenesis in a pigmented human tissue-cultured skin equivalent," *Indian J. Dermatol.*, vol. 64, no. 2, 2019. https://doi.org/10.4103/ijd.ijd_410_17.
[24] D. R. Gevaert, J., Chettle, "XRF analysis of strontium: Exploring cellulose as a soft tissue equivalent," *X-Ray Spectrom.*, vol. 48, no. (5), pp. 443–451, 2019. https://doi.org/10.1002/xrs.3025.
[25] F. A. Beaudoin Cloutier, C., Goyer, B., Perron, C., Gauvin, R., Auger, "In Vivo Evaluation and Imaging of a Bilayered Self-Assembled Skin Substitute Using a Decellularized Dermal Matrix Grafted on Mice," *Tissue Eng. - Part A*, vol. 23, no. (7-8), pp. 313–322, 2017. https://doi.org/10.1089/ten.tea.2016.0296.
[26] S. Michael *et al.*, "Tissue Engineered Skin Substitutes Created by Laser-Assisted Bioprinting Form Skin-Like Structures in the Dorsal Skin Fold Chamber in Mice," *PLoS One*, vol. 8, no. 3, 2013. https://doi.org/10.1371/journal.pone.0057741.
[27] M. Alssabbagh, A. A. Tajuddin, M. A. Manap, and R. Zainon, "Fabrication of a thyroid phantom for image quality in nuclear medicine using the 3D printing technology," *ARPN J. Eng. Appl. Sci.*, vol. 12, no. 9, 2017.
[28] Y.-N. Seol, Y., Kim, J., Kim, A., Choi, B.O., Kang, "Development of Tissue Equivalent Materials for a Multi-modality (CT&MRI) Phantom in MRI-guided Radiation Treatment," *J. Korean Phys. Soc.*, vol. 73, no. (7), pp. 1012–1018, 2018. https://doi.org/10.3938/jkps.73.1012.
[29] A. Haag, L.C., Jason, "Synthetic gelatins as soft tissue simulants," *AFTE J.*, vol. 52, no. (2), pp. 67–84, 2020.
[30] J. L. Hirsch, S.D., Powers, J.M., Rhodes, "Neonatal Soft Tissue Reconstruction Using a Bioengineered Skin Substitute," *J. Craniofac. Surg.*, vol. 28, no. (2), pp. 489–491, 2017. https://doi.org/10.1097/scs.0000000000003346.
[31] S. Joshi, P. K. Ajikumar, K. Sivasubramanian, and V. Jayaraman, "Synthesis, characterization and low energy photon attenuation studies of bone tissue substitutes," *J. Polym. Eng.*, vol. 40, no. (2), pp. 99–108, 2020. https://doi.org/10.1515/polyeng-2019-0179.
[32] S. Prabhu, S. G. Bubbly, and S. B. Gudennavar, "Synthetic polymer hydrogels as potential tissue phantoms in radiation therapy and dosimetry," *Biomed. Phys. Eng. Express*, vol. 6, no. (5), p. 05500, 2020. https://doi.org/10.1088/2057-1976/aba209.
[33] R. Singla, S. M. S. Abidi, A. I. Dar, and A. Acharya, "Nanomaterials as potential and versatile platform for next generation tissue engineering applications," *J. Biomed. Mater. Res. - Part B Appl. Biomater.*, vol. 107, no. 7, pp. 2433–2449, 2019. https://doi.org/10.1002/jbm.b.34327.
[34] V. P. Singh, N. M. Badiger, and H. R. Vega-Carrillo, "Neutron kerma factors and water equivalence of some tissue substitutes," *Appl. Radiat. Isot.*, vol. 103, 2015. https://doi.org/10.1016/j.apradiso.2015.05.014.
[35] B. C. Nascimento, A. Frimaio, R. M. M. Barrio, A. C. A. Sirico, and P. R. Costa, "Comparative analysis of the transmission properties of tissue equivalent materials," *Radiat. Phys. Chem.*, vol. 167, 2020. https://doi.org/10.1016/j.radphyschem.2019.04.050.
[36] R. Kargar Shaker Langaroodi, S. M. M. Abtahi, and M. E. Akbari, "Investigation of the radiological properties of various phantoms for their application in low energy X-rays dosimetry," *Radiat. Phys. Chem.*, vol. 157, 2019. https://doi.org/10.1016/j.radphyschem.2018.12.010.
[37] M. S. Saleh, H.H., Sharaf, J.M., Alkhateeb, S.B., Hamideen, "Studies on equivalent atomic number and photon build-up factors for some tissues and phantom materials.," *Radiat. Phys. Chem.*, vol. 165,108388, 2019. https://doi.org/10.1016/j.radphyschem.2019.108388.
[38] M. R. Hoerner, M. R. Maynard, D. A. Rajon, F. J. Bova, and D. E. Hintenlang, "Three-dimensional printing for construction of tissue-equivalent anthropomorphic phantoms and determination of conceptus dose," in *American Journal of Roentgenology*, 2018, vol. 211, no. 6. https://doi.org/10.2214/ajr.17.19489.
[39] D. R. Dance, S. Christofides, A. D. A. Maidment, I. D. McLean, K. H. Ng, and T. Editors, *Diagnostic Radiology Physics: A Handbook for Teachers and Students*. 2014.
[40] J. H. Hubbell and S. M. Seltzer, "NIST_ X-Ray Mass Attenuation Coefficients - Section 3 (Updated)." NIST, Gaithersburg, MD 20899, 2019.
[41] F. Zhang *et al.*, "Design and fabrication of a personalized anthropomorphic phantom using 3D printing and tissue equivalent materials," *Quant. Imaging Med. Surg.*, vol. 9, no. 6, pp. 94–100, 2019. https://doi.org/10.21037/qims.2018.08.01.
[42] S. Noblet, C., Delpon, G., Supiot, S., Paris, F., Chiavassa, "A new tissue segmentation method to calculate 3D dose in small animal radiation therapy," *Radiat. Oncol.*, vol. 13, no. (1), p. 32, 2018. https://doi.org/10.1186/s13014-018-0971-8.
[43] ICRP, "Conversion Coefficient for use in Radiological Protection against External Radiation: P74," *ICRP Publication 74, Ann. ICRP 26(3-4)*. ICRP, 1996https://doi.org/10.1016/s0146-6453(96)90003-2.
[44] M. R. Hoerner, M. R. Maynard, F. J. Bova, D. E. Hintenlang, R. Da, and B. Fj, "Three-Dimensional Printing for Construction of Tissue-Equivalent Anthropomorphic Phantoms and Determination of Conceptus Dose," *Med. Phys. Informatics*, vol. 211, no. December, pp. 1283–1290, 2018. https://doi.org/10.2214/ajr.17.19489.
[45] E. Meyer-scott, C. Silberhorn, and A. Migdall, "Single-photon sources: Approaching the ideal through multiplexing Single-photon sources: Approaching the ideal through multiplexing," *Rev. Sci. Instrum.*, vol. 041101, no. April, 2020. https://doi.org/10.1063/5.0003320.

APPENDIX A
PHOTON CREATION DATA FROM MCNPX SIMULATION

MeV	Bremsstrahlung	Positron Annihilation	1st Fluorescence	2nd Fluorescence	*g-factor
0.040	1.70E-04	0	2.14E-03	0	0.057851
0.050	2.67E-04	0	2.15E-03	0	0.0483038
0.060	3.84E-04	0	2.15E-03	1.66E-12	0.04227767
0.070	5.20E-04	0	2.16E-03	0	0.03823286
0.072	5.50E-04	0	2.16E-03	0	0.03758875
0.074	5.79E-04	0	2.16E-03	0	0.03698635
0.076	6.10E-04	0	2.16E-03	0	0.03642467
0.078	5.28E-04	0	5.17E-02	0.0016791	0.69170615
0.080	5.37E-04	0	5.18E-02	0.0016799	0.6748465
0.082	5.46E-04	0	5.18E-02	0.0016807	0.65879317
0.084	5.57E-04	0	5.18E-02	0.0016814	0.64350101
0.086	5.68E-04	0	5.18E-02	0.0016821	0.62888233
0.088	5.80E-04	0	5.19E-02	0.0016826	0.61491125
0.090	5.92E-04	0	5.19E-02	0.0016831	0.60157167
0.092	6.06E-04	0	5.19E-02	0.0016837	0.58883413
0.094	6.21E-04	0	5.19E-02	0.0016843	0.57667968
0.096	6.36E-04	0	5.19E-02	0.0016851	0.56507427
0.098	6.52E-04	0	5.20E-02	0.001686	0.55400398
0.100	6.70E-04	0	5.20E-02	0.0016871	0.54342705
0.105	7.16E-04	0	5.21E-02	0.0016906	0.51902619
0.110	7.68E-04	0	5.22E-02	0.0016943	0.49694645
0.115	8.25E-04	0	5.22E-02	0.0016938	0.4757167
0.120	8.86E-04	0	5.22E-02	0.0016932	0.45628833
0.125	9.53E-04	0	5.22E-02	0.0016926	0.43844372
0.130	1.02E-03	0	5.21E-02	0.001692	0.42200077
0.135	1.10E-03	0	5.21E-02	0.0016913	0.40679407
0.140	1.18E-03	0	5.21E-02	0.0016906	0.39269571
0.145	1.26E-03	0	5.21E-02	0.0016898	0.37959241
0.150	1.35E-03	0	5.21E-02	0.001689	0.367376
0.200	2.44E-03	0	5.18E-02	0.0016798	0.279704
0.300	5.33E-03	0	5.08E-02	0.001645	0.19267333
0.400	8.50E-03	0	4.86E-02	0.0015698	0.14661388
0.500	1.15E-02	0	4.53E-02	0.0014613	0.1164876
0.600	1.43E-02	0	4.18E-02	0.0013476	0.0957335
0.800	1.96E-02	0	3.61E-02	0.0011598	0.07105538
1.000	2.50E-02	0	3.22E-02	0.0010301	0.0582366
1.250	3.25E-02	0.00403995	2.93E-02	0.00093462	0.05338126
1.500	4.07E-02	0.020288	2.85E-02	0.00090674	0.06024783
2.000	6.03E-02	0.066372	3.02E-02	0.00095915	0.07894732
3.000	1.16E-01	0.154755	3.86E-02	0.00122	0.103375
4.000	1.95E-01	0.225925	4.91E-02	0.0015508	0.11787583
6.000	4.29E-01	0.33057	7.22E-02	0.002273	0.13899783
8.000	7.63E-01	0.406625	9.6JE-02	0.0030219	0.15856024
10.000	1.19E+00	0.46791	1.20E-01	0.0037781	0.17832181
15.000	2.63E+00	0.5904	1.80E-01	0.00565015	0.22694534

*Estimated data using equation 1